Supplemental Figure 1.

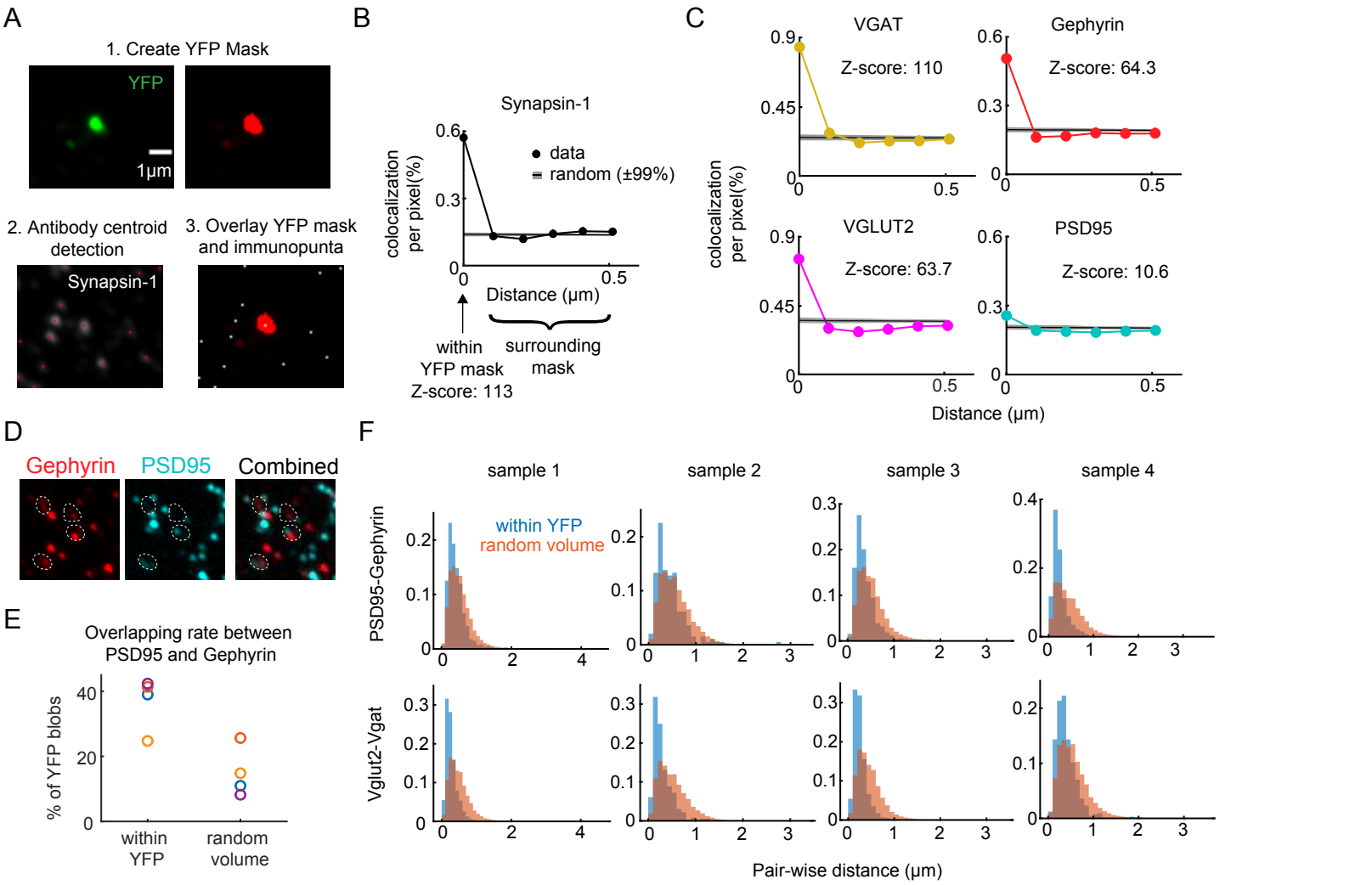

Supplemental Figure 2.

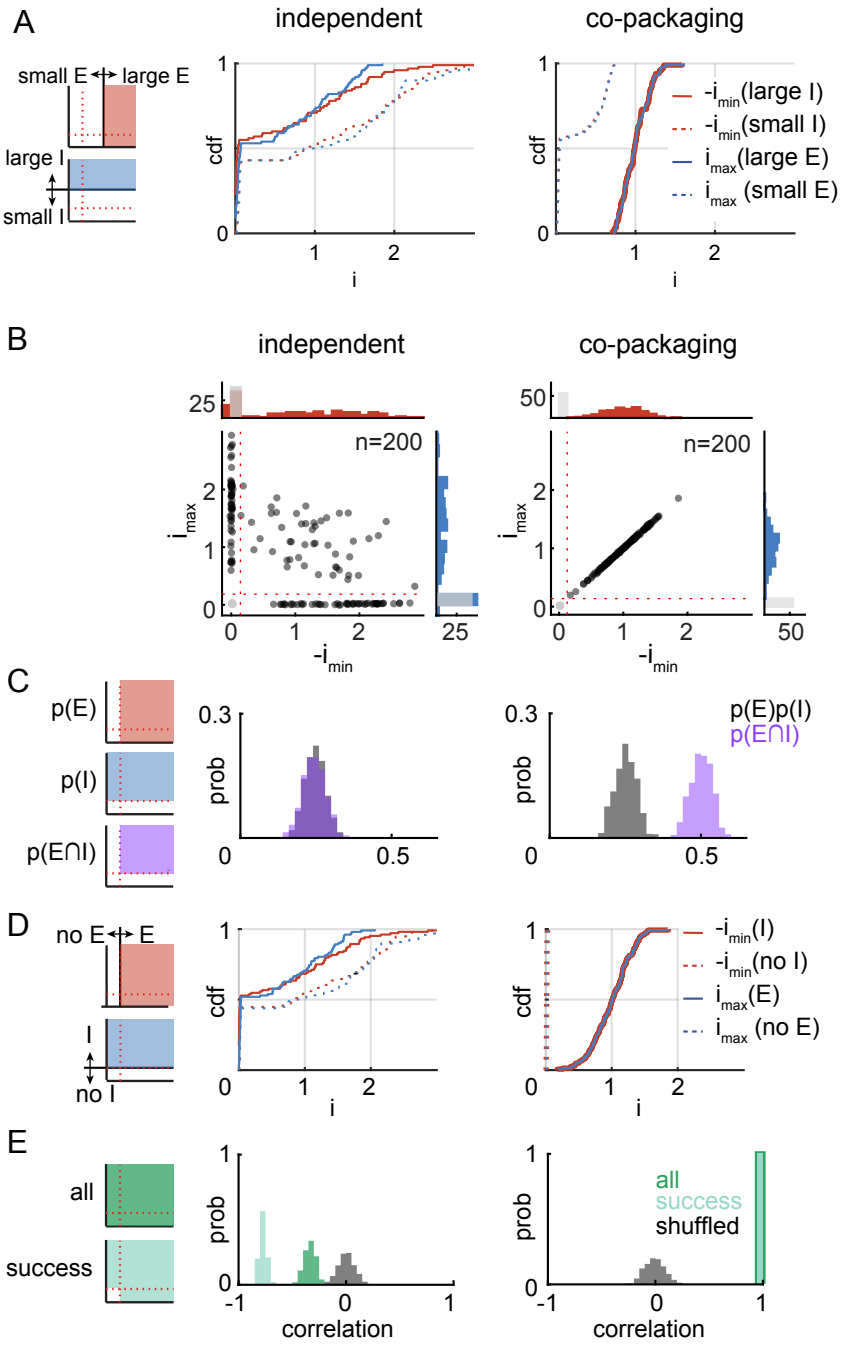

Supplemental Figure 3.

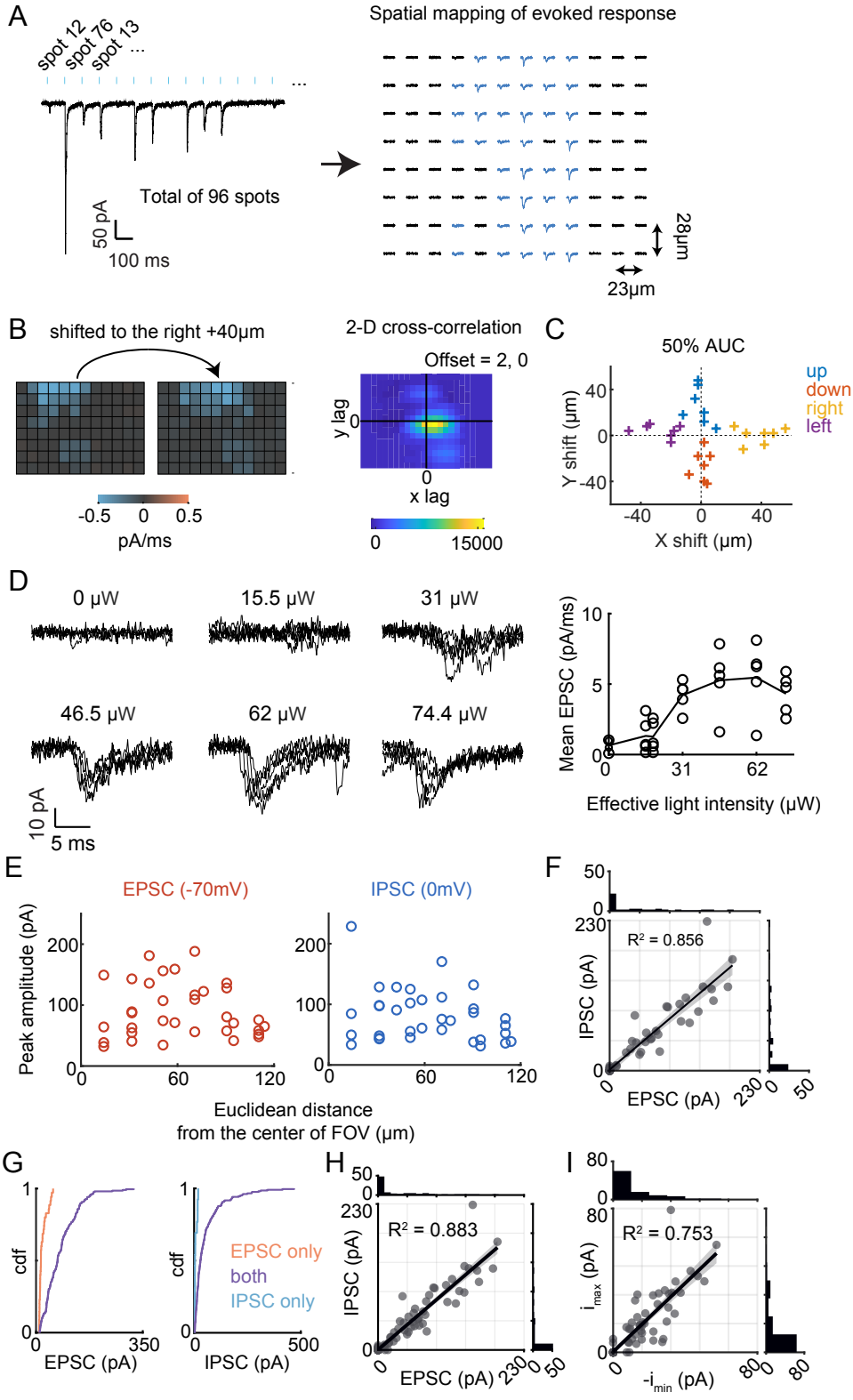

Supplemental Figure 4.

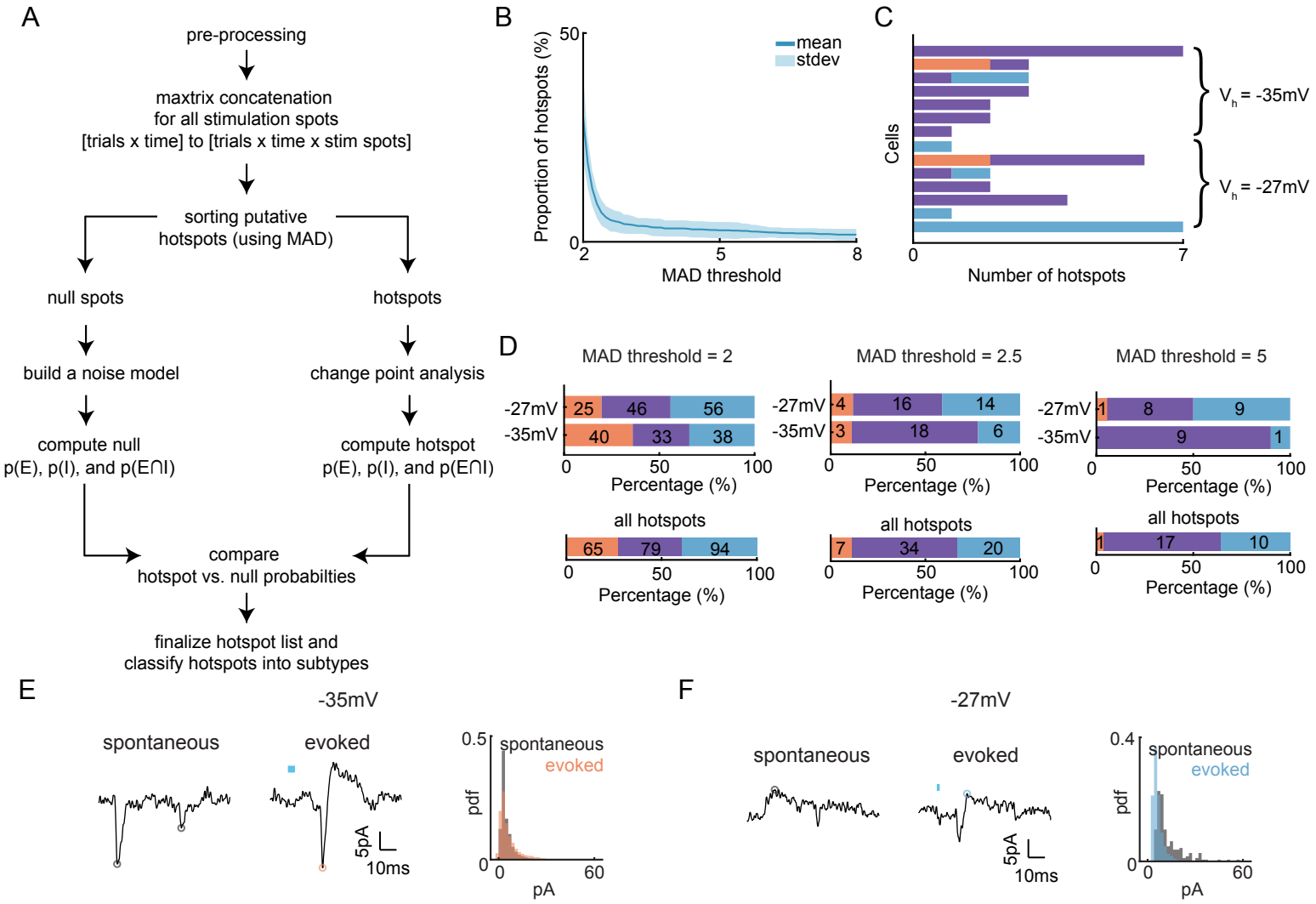

Supplemental Figure 5.

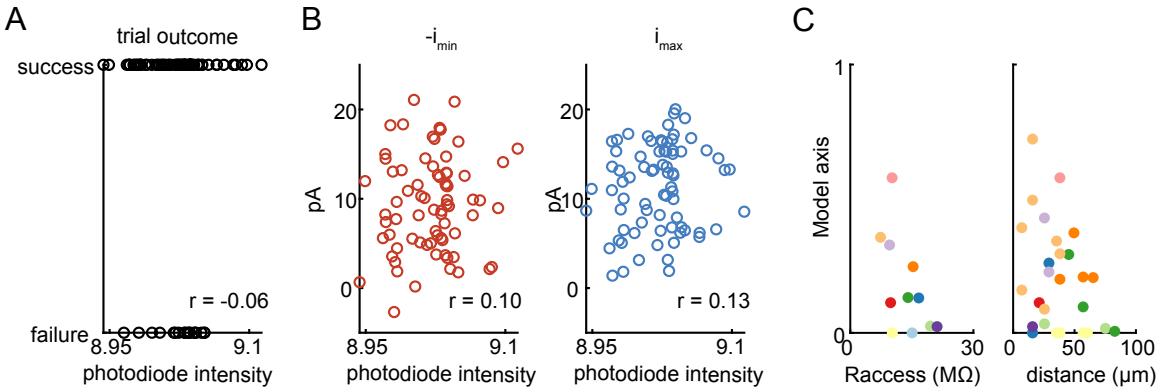

Supplemental Figure 6.

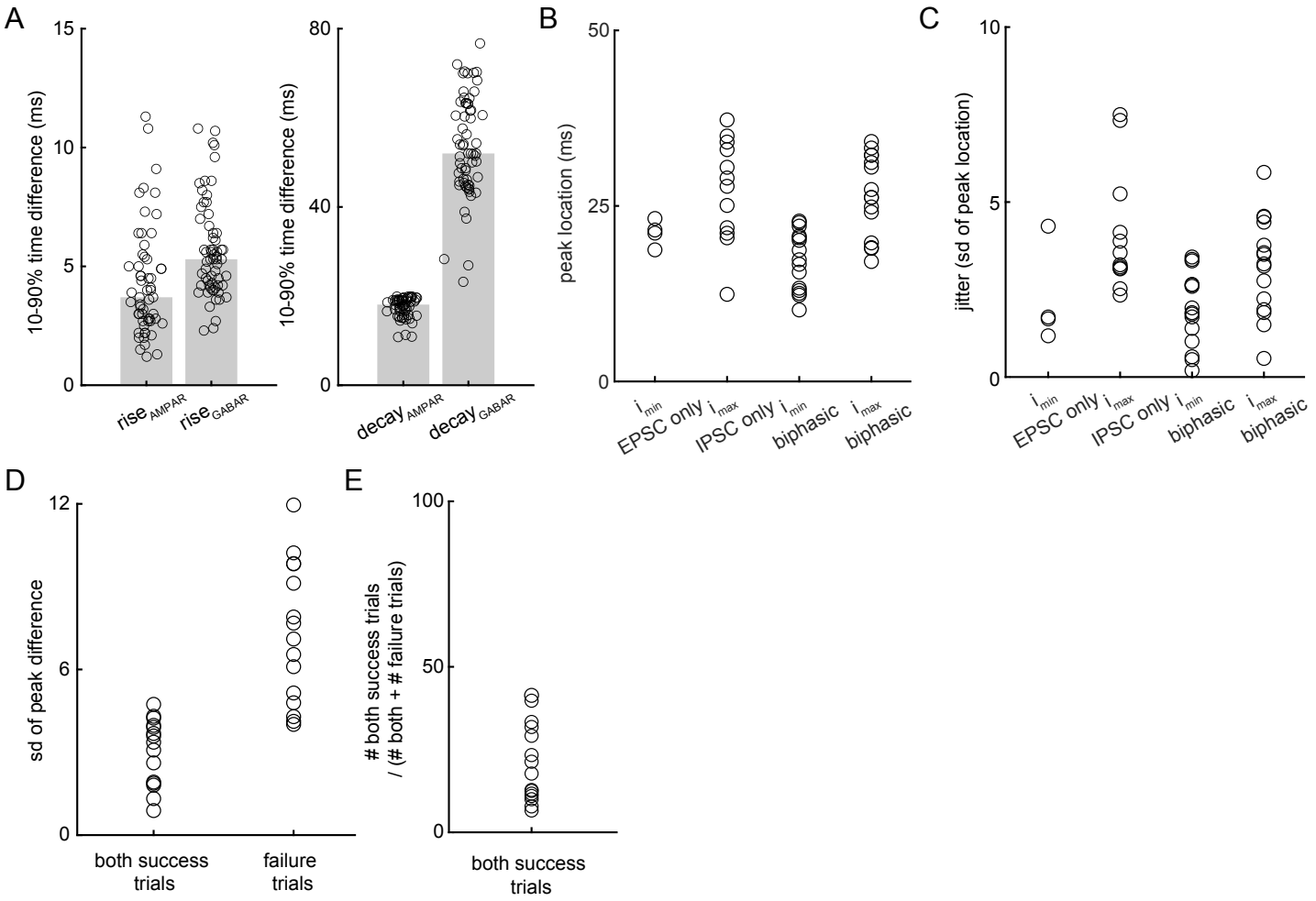

Supplemental Figure 7.

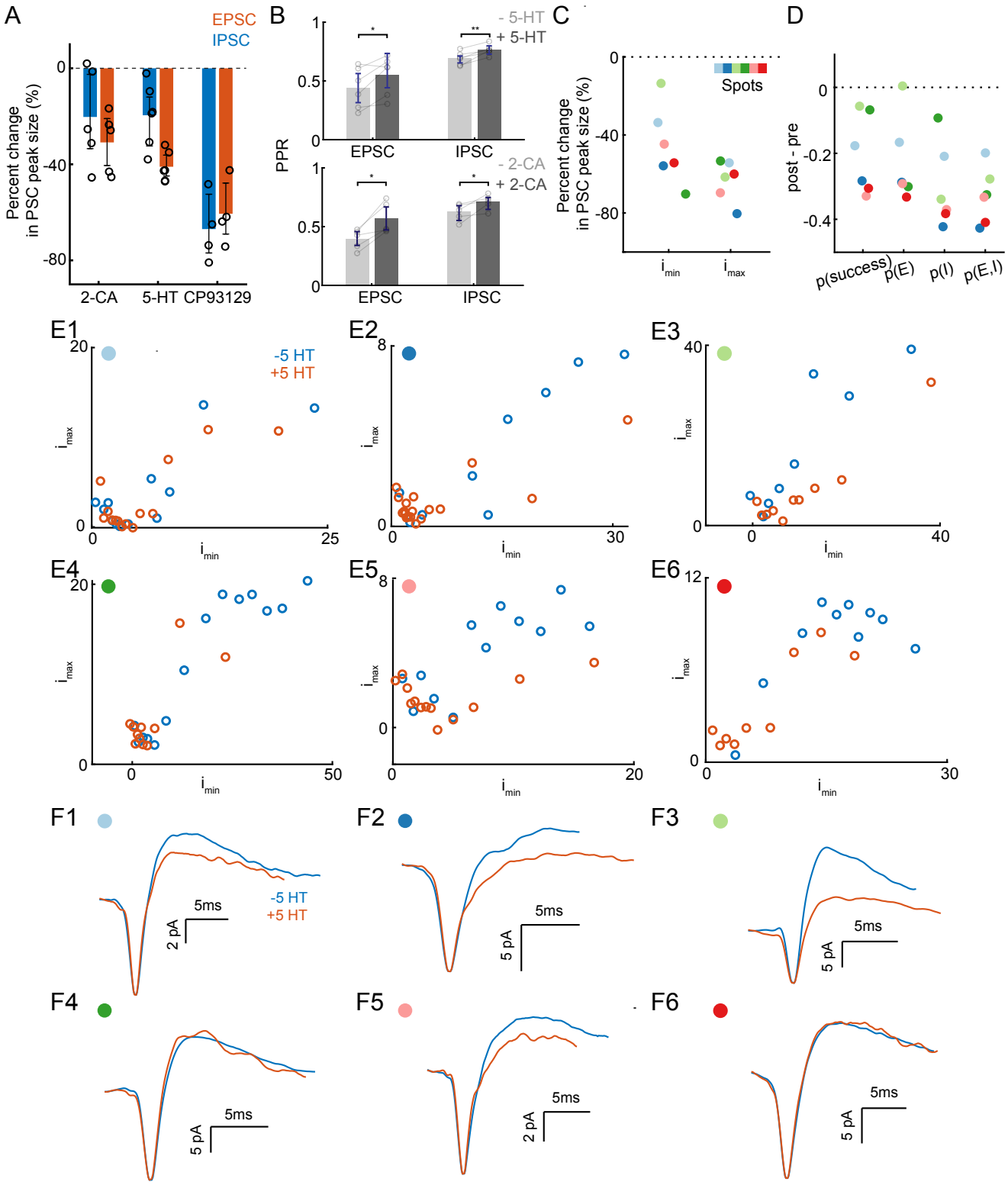

Supplemental Figure 8.

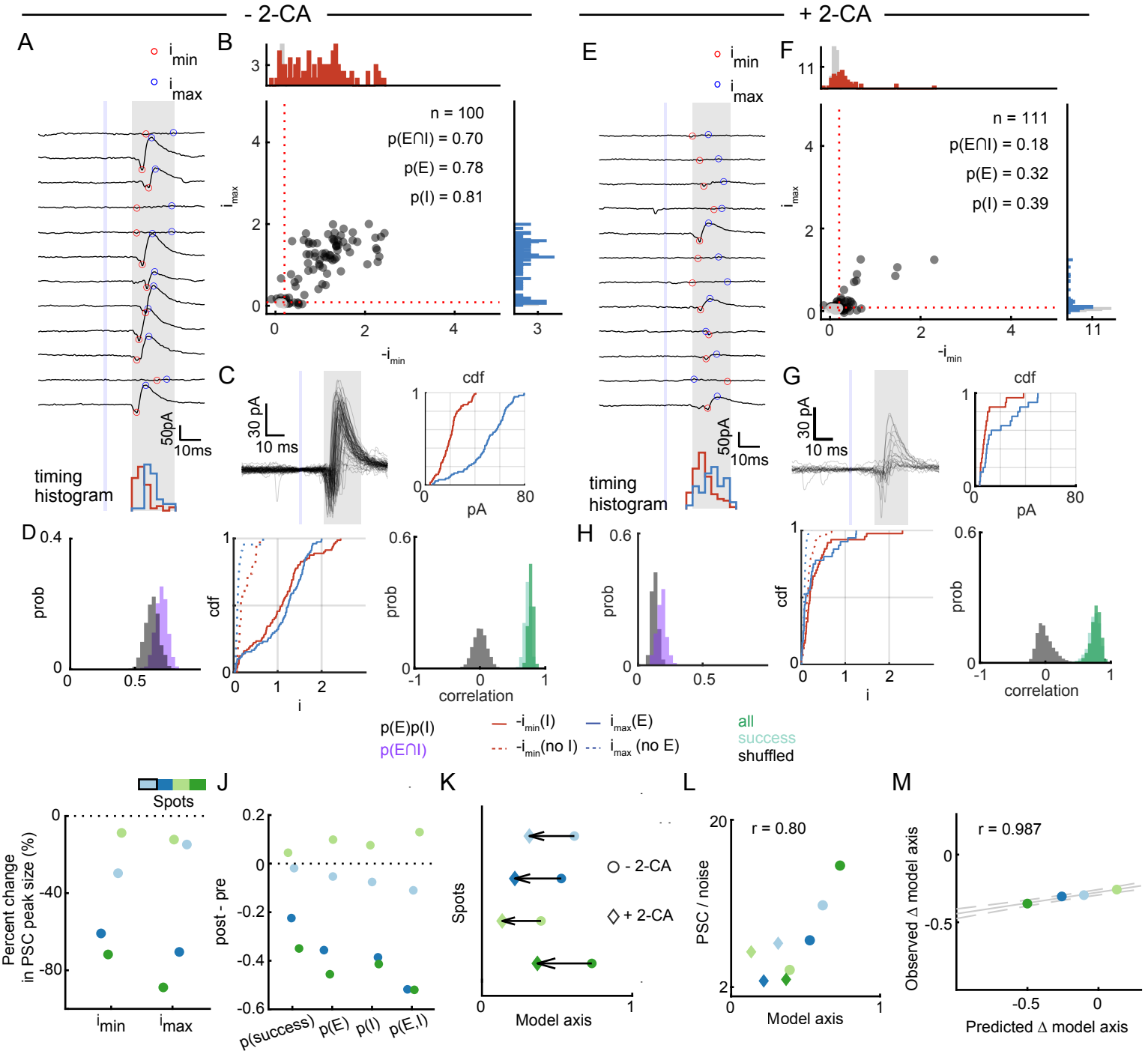

SFig. Legends

SFig. 1. Co-localization analysis of antibodies within and outside of YFP-labelled EP Sst+ terminals. Related to Fig. 1

A) Co-localization analysis schematic. The YFP channel fluorescence was used to create masks to identify pixel regions containing labeled *Sst+* terminals. Each antibody channels was analyzed independently to extract the locations of the centroids of immunolabeled puncta. Extracted centroid locations were compared to the YFP masks in the same sample plane. For each immunolabeling channel, the percentage of pixels in the YFP+ masks that contained a punctum centroid was calculated and is referred to as the "co-localization" metric.

B) Example synapsin-1 immunopuncta co-localization within the YFP mask and the surrounding regions compared to that expected by chance. Antibody locations were randomized 1000 times and the 99th percentile upper and lower boundaries are shown. Z-score is calculated as the difference between the mean antibody co-localization within the YFP mask and the mean randomized co-localization, divided by the standard deviation of the random co-localization.

C) Example co-localization analysis results for Vgat, Gephyrin, Vglut2, and PSD95 antibodies from the tissue sample shown in B.

D) Enlarged images of the inset in Fig 1C demonstrating colocalization in YFP-labelled *Sst+* terminals and the postsynaptic proteins for scaffolding of GABA (Gephyrin) and glutamate (PSD95) ionotropic receptors.

E) Overlapping rate of Gephyrin and PSD95 immunopuncta inside the same YFP blobs compared to a random volume of similar area size.

F) Paired distances between Gephyrin-PSD95 (top) and Vglut2-Vgat (bottom) puncta pairs within YFP volumes and random volumes.

SFig. 2. Accurate separation of synaptic failures is not required for the cdf analysis. Related to Fig. 2

A) Simulated cdfs of maximum PSC amplitudes (i_{max}, blue) given a large (i_{max}(E), solid) or small (i_{max}(no E), dashed) excitatory current in the same trial for the independent (*left*) and co-packaging (*right*) release models. Similar analyses were performed for the minimum PSC

amplitudes ($-i_{min}$, red) given large ($-i_{min}(I)$, solid) or small ($-i_{min}$(no I), dashed) inhibitory currents in the same trial. Simulation parameters are the same as in Fig 2D. Here we used the median to separate currents into large and small.

B-E) Simulation results as in Fig. 2C-F with colored noise (3kHz corner frequency Bessel filtered).

SFig. 3. DMD based photo-stimulation enables spatially-specific activation of EP *Sst+* OChIEF-expressing terminals. Related to Fig. 3

A) *left*, Each trial consisted of rapid serial illumination of 23 x 28 µm photo stimulation spots to 96 different locations tiling the field of view in a pseudorandom spatial pattern such that the PSCs evoked from each spot are recorded in ~10s voltage-clamp trace. Shown here is an example recording at -70 mV. *right,* The 96 PSCs in each trace are extracted and assigned to spatial locations based on the coordinates of the illuminated spots and the stimulus timing.

B) Example showing that the DMD-evoked spatial map is consistent with the physical locations of EP *Sst+* terminals. *left,* the input-output relationship was initially mapped (V_h=-70mV) using the DMD-based optogenetic stimulation platform then the brain slice was shifted in +x direction relative to the microscope objective lens by 40 µm after which the input-output relationship was re-mapped. *right*, 2D cross-correlation of the two spatial maps (before and after the objective lens movement) reveals that the two images are offset by 2 pixels, as predicted by the pixel spacing. The offset is calculated from the X and Y locations where the cumulative sums of correlation coefficient across y and x, respectively, reach the 50% of the total sum. Spatial maps are calculated from the average of 5 trials.

C) Summary of quantification of cross-correlation calculated shifts as described in (B) for 7 cells from 3 animals. Colors indicate the direction of the slice movement.

D) Saturation of the amplitude of the evoked PSC from the same 23 x 28 µm photo-stimulation spot in an example LHb neuron. *left,* electrophysiological recording (V_h=-70 mV) for 5 trials at each indicated light intensity. Traces correspond to 5-25 ms time window after stimulation onset. *right,* Individual (circle) and average (line) EPSC amplitudes as a function of illumination intensity.

E) Relationship between distance of the stimulation spots from the LHb cell body (located at the center of field of view (FOV)) and the corresponding evoked EPSC (*left*) and IPSC (*right*) peak amplitudes (data shown for the same neuron as in Fig 3F).

F) Scatterplot of IPSC vs. EPSC peak amplitude pairs evoked at photo-stimulated spots within 80 µm perimeter from the center of the field of view from the neuron analyzed in Fig 3F.

G) Cdfs comparing the EPSC and IPSC amplitude distributions in different classes of hotspots. EPSC-only (*left,* orange) and IPSC-only (*right*, blue) hotspots have smaller amplitudes than do co-transmission hotspots (purple).

H) Scatterplot of IPSC vs. EPSC amplitudes evoked at each spot for an example LHb neuron. The IPSC/EPSC amplitude ratio is conserved across multiple sets of EP *Sst+* axons synapsing onto the same postsynaptic cell. The top and right histograms show the distributions of EPSC and IPSC amplitudes, respectively. Fitted line: $y = 0.438 + 0.856x$.

I) Scatterplot of i_{max} and i_{min} at V_h=-35 mV for the trace shown in Fig 3E. The top and right histograms show the distributions of $-i_{min}$ and i_{max}, respectively. Fitted line: $y = 0.316 + 0.955x$.

SFig. 4. Automated analysis of evoked unitary responses. Related to Fig. 4

A) Hotspot detection and classification analysis pipeline flowchart (see Methods).

B) Effect of median absolute deviation (MAD) threshold on the proportion of putative hotspots out of total stimulation spots. The MAD threshold, expressed in multiples of the empirically measured MAD for each cell, determines the selection of putative active hotspots which are required to have current deviation that exceed the threshold at least 5ms (the branching step in panel A). Mean and standard deviation of the proportion of illuminated spots designated as hotspots (data from 14 cells are shown). A MAD threshold of 3 was used for Fig. 4F.

C) Distribution of putative hotspot numbers across all cells (n=14 cells, 9 animals). MAD threshold of 3 was used. The holding potential of individual cells is indicated. PSCs are designated as EPSCs only (red), IPSCs only (blue), or both (purple).

D) Effect of MAD threshold on the proportion of final hotspot subtypes. As in Fig. 4F for MAD threshold of 2 (*left*), 2.5 (*middle*), and 5 (*right*). Color code as in (C).

E) Spontaneous EPSCs (*left*) and unitary evoked biphasic PSC (*middle*) recorded from the same cell with evoked EPSC amplitude indicated. *right*, Histograms of amplitudes of spontaneous EPSCs (gray, median amplitude 95% CI=3.37-3.50 pA, median frequency=8.9 Hz; 14 cells, 9 animals) and evoked EPSCs measured in a subset of cells with unitary biphasic PSCs (orange, median amplitude 95% CI=3.82-4.17 pA; 11 cells, 6 animals).

F) As in panel E for a spontaneous and unitary evoked IPSCs. The spontaneous IPSCs (gray) had median amplitude 95% CI=9.15-10.51 pA and frequency=0.2 Hz whereas the evoked IPSCs (blue) had median amplitude 95% CI =3.84-4.18 pA.

SFig. 5. Control analyses for unitary biphasic PSCs. Related to Fig. 5

A-B) Stimulation intensity fluctuation as detected by a photodiode versus trial-by-trial outcome (A)amplitudes of $-i_{min}$ and i_{max} (B). Same dataset as in Fig. 5F)-J).

C) Average model feature indicators for individual spots vs. access resistance (*left*) and Euclidean distance of stimulation site from the center of FOV (*right*). Same dataset as in Fig. 6E).

SFig. 6. Receptor kinetics and jitter analysis. Related to Fig. 4

A) Rise (*left*) and decay (*right*) times of the AMPAR- and $GABA_A$R-mediated postsynaptic currents. Recordings in presence of 10 µM CPP at Vh=-64mV and 10mV. Time difference between 10% and 90% of peak was measured for rise and decay of each stimulated spots that evoked PSCs larger than 30pA.

B) Maximum and minimum peak location from the stimulation onset of EPSC only, IPSC only, and both hotspots in Fig. 4F.

C) Jitter of maximum and minimum peaks in EPSC only, IPSC only, and both hotspots from Fig. 4F.

D) Standard deviation of maximum and minimum peaks in both hotspots from Fig. 4F.

E) Proportion of both success trials relative to the total trial number shown in D).

SFig. 7. Activation of serotonin and adenosine receptors affect glutamate/GABA co-release from EP *Sst*+ terminals in LHb. Related to Fig. 7

A) Peak amplitude changes in the DMD ring stimulation evoked composite EPSC (-64 mV) and IPSC (10 mV) as result of 2-CA (100 μM), 5-HT (1 μM), and CP93129 (1 μM). Each circle represents the difference in mean evoked peak amplitude of 15 trials before and after each drug application. Bars and error bars indicate the mean and bootstrapped 95% confidence interval of the mean, respectively.

B) Normalized paired-pulse ratios before and after bath application of 5-HT (*top*) and 2-CA (*bottom*). Bars and error bars indicate the mean and bootstrapped 95% confidence interval of the mean, respectively. Asterisks represent significance level of paired t-test comparing before and after conditions.

C) Average relative minimum and maximum amplitude changes of DMOS-evoked unitary biphasic spots across all trials as result of 5-HT bath application. Colors indicate spot identity consistent as in Fig. 7O.

D) Changes in probabilities of detecting success trials, EPSC, IPSC, and both trials due to 5-HT bath application for DMOS-stimulated unitary biphasic spots. Each dot represents the difference in probabilities calculated from scatterplot of each spot before and after 5-HT. Colors and markers are consistent as in panel C.

E) The effect of 5-HT on subset distributions of minimum and maximum amplitudes of co-packaging sites, without sorting trials by success and failures. Scatter corresponds to the amplitudes of the average trace of different subsets of dataset before (blue) and after (red) 5-HT bath application. Each dot in the top right indicates spot identity consistent as in Fig. 7O.

F) The effect of 5-HT on the average waveform of co-packaging sites, without sorting trials by success and failures. Average of each trial was aligned by the minimum peak location within the analysis time window. Before (blue) and after (red, normalized by the minimum peak amplitude of "before" condition) 5-HT bath application traces are compared. Each dot in the top right indicates spot identity as in Fig. 7O.

SFig. 8. 2-CA reduces p_r of glutamate and GABA while maintaining their co-packaging. Related to Fig. 8

A-D and E-H) As in Fig. 7E-H and I-L for optically-evoked PSCs from a hotspot consistent with the co-packaging model before (A-D) and after (E-H) application of 2-CA (100 µM)

I) Average relative $-i_{min}$ and i_{max} changes across all trials as result of 2-CA application. Colors indicate spot identity.

J) Changes in probabilities of success, EPSC, IPSC, and both trials due to 2-CA application for DMOS-stimulated biphasic spots. Colors as in panel I.

K-M) As in Fig. 8C-E for the 2-CA effects (n=4) on PSCs from hotspots consistent with the co-packaging model before 2-CA application

Supplemental Tables

Supplemental Table 1. Summary of 5-HT effect on six example co-packaging unitary PSC sites, Related to Fig. 7. Spot annotated with * corresponds to Figure7E-L.

spot	Caveats	Sample size of biphasic trials (before/ after)	Proportion of rejecting null (bootstrapped K-S test) "both" success trials	Proportion of rejecting null (bootstrapped K-S test) all success trials	Mean amplitude (in pA)	Model axis value change (post-pre)	PSC / noise change (post-pre)
*		(52/25)	0.5305(E); 0.3076 (I)	0.5992 (E); 0.8139 (I)	before: 13.5 (E), 14.8 (I); after: 10.4 (E), 13.4 (I)	-0.351	-2.024
	p(I) drops to 0.18 after 5-HT and the spontaneous activity makes cdf difference smaller	(47/18)	0.1616(E); 0.1627 (I)	0.9933 (E); 0.9999 (I)	before: 19.6 (E), 6.83 (I); after: 16.7 (E), 6.30 (I)	-0.585	-3.788
	p(E∩I) reduction could be mostly	(41/23)	0.2257(E); 0.2132 (I)	0.5929 (E); 0.9989 (I)	before: 15.2 (E), 30.7 (I);	-0.341	-2.846

	driven by p(I) reduction				after: 19.4(E), 32.7 (I)		
●	Putative co-packaging double synapse (smaller cluster and larger cluster)	(107/49)	0.998 (E); 0.9712 (I)	1 (E); 1 (I)	before: 19.7 (E), 15.1 (I); after: 9.41 (E), 11.0 (I)	-0.383	-5.392
●		(58/18)	0.1575 (E); 0.245 (I)	0.8604 (E); 0.9147 (I)	before: 10.0 (E), 7.62 (I); after: 9.80 (E), 6.67 (I)	-0.282	-1.324
●	Putative multivesicular release site	(83/34)	0.996 (E); 0.5939 (I)	0.9988 (E); 0.9732 (I)	before: 16.4 (E), 10.2 (I); after: 11.4 (E), 8.58 (I)	-0.0224	-3.488